Astron. Astrophys. 325, 791–802 (1997)

ASTRONOMY
AND
ASTROPHYSICS

The effect of spatially dependent heating on the thermal equilibria of coronal loops

César A. Mendoza-Briceño[1,2] **and Alan W. Hood**[1]

[1] Mathematical Institute, University of St. Andrews, St. Andrews, KY16 9SS, UK
[2] Centro de Astrofísica Teórica, Facultad de Ciencias, Universidad de los Andes, Mérida, Venezuela

Received 2 August 1996 / Accepted 26 March 1997

Abstract. The thermal equilibria along a symmetric coronal loop with constant cross-sectional area is investigated in the absence of gravity. A coronal heating function that depends on distance along the loop is considered and the effects of varying the values of the parameters involved in the governing equations are studied. It is found that there is a critical decay length of the heating below which a hot coronal loop does not exist. It is suggested that thermal non-equilibrium occurs, allowing the existence of catastrophic cooling and it is shown that prominence-type equilibria are possible. A study of the stability of the equilibrium up to a second order approximation is presented, and it is found that the response of the structure not only depends on the amplitude of the disturbance, but also on whether the disturbance increases or decreases the equilibrium temperature.

Key words: Sun: corona – Sun: magnetic fields – Sun: prominences – stars: coronae

1. Introduction

Observations in X-ray and EUV have shown that the solar corona consists of a large number of loops which outline the coronal magnetic field in form of magnetic flux tubes that confine the plasma. Often these loops are observed to form arcades and other structures. Also, these coronal loops possess lifetimes which are frequently greater than the timescales defined by thermal conduction and radiation losses. This suggests that coronal loops exist in a quasi-static state in the presence of some form of steady energy input. In consequence, static models of coronal loop structures have been proposed in which the mechanical energy deposited into each volume element is exactly balanced by a radiative loss flux and conductive energy flux into (or out of) the element.

Since energy or mass transport across the loop is strongly inhibited by the magnetic field thermal conduction is assumed to take place only along the field lines.

Send offprint requests to: C.A. Mendoza-Briceño[2]

Rosner, et al (1978), using an order of magnitude analysis, derived scaling laws between the loop length (L), the plasma pressure (p), and the maximum temperature (T_s) along the loop. They assumed that the base conductive flux vanishes at a particular temperature and the flux also vanishes at the loop summit, from symmetry arguments. The scaling laws derived have the form

$$T_s \approx 1.4 \times 10^3 (pL)^{1/3},$$

for the summit temperature and the heating

$$h \approx p^{7/6} L^{-5/6}.$$

Craig et al (1978) also demonstrated that a relationship must exist between the thermodynamic properties of a loop and its length, when the pressure is constant, of the form

$$T_s^{9/4} \approx N_s L,$$

where N_s is the number density.

Hood and Priest (1979) solved the problem of thermal equilibrium along a coronal loop when gravity is neglected. They found the existence of cool solutions with summit temperatures below 10^5 K when either the external gas pressure p, or the length L of the field lines increases (due to motions of the footpoints) or the heating decreases and suggest that they may explain the existence of active region prominences.

Priest and Smith (1979) applied these techniques to an arcade consisting of a succession of loops. Gravitational effects were considered by Vesecky et al (1979), Wragg and Priest (1981a,b; 1982), Serio et al. (1981), She et al. (1986), Steele and Priest (1994), Mendoza-Briceño (1996).

Hood and Anzer (1988) studied the problem of thermal equilibrium qualitatively. They used a phase plane diagram approach to identify the different types of solution that are possible. The advantage of this technique was that their conclusions were not sensitive to the actual choice of boundary condition adopted, which only determines the actual contour.

Steele and Priest (1990) confirmed and extended the work of Hood and Anzer (1988) by seeking numerical solutions to the different types of loops and determined the parameter regimes

for which they exist. Four different kinds of loops may exist, namely hot loops, warm loops, hot-cool loops and cool loops. They defined regions of the parameter space in which each type of solution occurs depending on both a physical parameter related to the length of the loop and the heating. Regions with only one solution have either a hot or a cool solution; two solution regions have one hot and one hot-cool; a three solution region has one hot solution, one warm and one cool solution. There are also regions in the solution space with no physically realistic solutions.

More recently, van den Oord and Zuccarello (1996) examined several aspects of the theory of coronal loop modelling and related the results to the observed differential emission measure (DEM).

In the present paper, our attention is focussed on investigating how the thermal equilibrium is effected when the heating function has a spatial dependence.

2. Equation of thermal equilibrium and boundary conditions

The equations for a static coronal loop can be written as

$$\frac{dp}{ds} = -\frac{\tilde{\mu}p}{\mathscr{R}T}g(s), \tag{1}$$

$$\frac{d}{ds}\left(\kappa\frac{dT}{ds}\right) = \left(\frac{\tilde{\mu}p}{\mathscr{R}}\right)^2 \chi T^{\alpha-2} - h(p,T,s), \tag{2}$$

where s represents the distance along the loop, $g(s)$ is the component of gravity along the loop, p is the gas pressure, T is the plasma temperature, h is the unknown heating function that may depend on p, T and s, and κ is the coefficient of thermal conduction (i.e. $\kappa \approx 10^{-11}T^{5/2}$ Wm^{-1}K^{-1} Spitzer (1962)). The first term on the right-hand side of Eq. (2) is the radiative loss term, where $\chi T^{\alpha-2}$ is the piecewise continuous function with χ and α given by Hildner (1974).

Eq. (1) expresses the balance between gravity and the pressure gradient along the loop, and Eq. (2) represents the balance between the energy gain due to coronal heating, the losses due to radiation, and the gains or losses due to thermal conduction.

Eqs. (1) and (2) can be written in dimensionless form by setting

$$\tilde{s} = s/L_0, \qquad \tilde{T} = T/T_0 \qquad \text{and} \qquad \tilde{p} = p/p_0 \tag{3}$$

in which T_0, p_0 are taken at typical coronal or chromospheric values, and L_0 is the half-length of the loop. Therefore

$$\frac{d\tilde{p}}{d\tilde{s}} = -\frac{\tilde{p}}{\tilde{T}}\tilde{g}(\tilde{s}), \tag{4}$$

$$\frac{d}{d\tilde{s}}\left(\tilde{T}^{5/2}\frac{d\tilde{T}}{d\tilde{s}}\right) = L_*^2\left[\tilde{p}^2\tilde{\chi}\tilde{T}^{\alpha-2} - \tilde{h}\right], \tag{5}$$

where

$$\begin{aligned}
\tilde{g}(\tilde{s}) &= \frac{\tilde{\mu}L_0}{\mathscr{R}T_0}g(s),\\
L_*^2 &= L_0^2\frac{\tilde{\mu}^2p_0^2\chi_0T_0^{\alpha_0-11/2}}{\mathscr{R}^2\kappa_0},\\
\tilde{h} &= \frac{\mathscr{R}^2h(\tilde{p},\tilde{T},\tilde{s})}{\tilde{\mu}^2p_0^2\chi_0T_0^{\alpha_0-2}},\\
\tilde{\chi} &= \frac{\chi T_0^{\alpha}}{\chi_0T_0^{\alpha_0}}.
\end{aligned} \tag{6}$$

In order to solve Eqs. (4) and (5), boundary conditions must be provided. It is assumed that the temperature $\tilde{T} = \tilde{T}_b$ and pressure $\tilde{p} = \tilde{p}_b$ at the footpoints of the loop are fixed and by symmetry, there is a zero temperature gradient at the loop summit. There are other choices of boundary conditions for example $d\tilde{T}/d\tilde{s} = 0$ at the base with $\tilde{p}_b$ adjusting to the value necessary for a solution to exist (Vesecky et al 1979, Rosner et al 1978). Since the mechanism of coronal heating $\tilde{h}$ is unknown, its form is assumed to be

$$\tilde{h} = h_* \exp\left(-\frac{1-\tilde{s}}{s_*}\right), \tag{7}$$

where $\tilde{s} = 1$ corresponds to the base of the loop (footpoint) and the dimensionless parameters h_* and s_* are given by

$$\begin{aligned}
h_* &= \frac{R^2h_0}{\tilde{\mu}^2p_0^2\chi_0T_0^{\alpha_0-2}},\\
s_* &= \frac{s_H}{L_0},
\end{aligned} \tag{8}$$

where s_H is the scale length of the heating.

This form of the heating mechanism represents waves that are damped in the corona and the amount of energy supplied to the loop will decay from the footpoint towards the summit.

In (4) the equation for $\tilde{g}(\tilde{s})$ denotes the ratio of loop length to base scale height. For typical loop heights and temperatures, the gravitational scale height $\Lambda = \mathscr{R}T_0/\tilde{\mu}g_0$ (g_0 is the solar surface gravity constant) is large compared to the size of the loop structure then, if

$$\tilde{g} \ll 1, \tag{9}$$

the force balance equation (1) reduces to the result that the pressure is approximately constant throughout the loop, and, therefore, the plasma structure is only determined by energy balance.

So, with gravity neglected Eq. (5) simplifies to

$$\frac{d}{ds}\left(T^{5/2}\frac{dT}{ds}\right) = L_*^2\left[p^2\chi T^{\alpha-2} - h_*\exp\left(\frac{1-s}{s_*}\right)\right], \tag{10}$$

where all tildes have been removed for convenience. In this equation three dimensionless parameters are involved namely L_*, the ratio of the conduction to radiation timescales, h_*, the

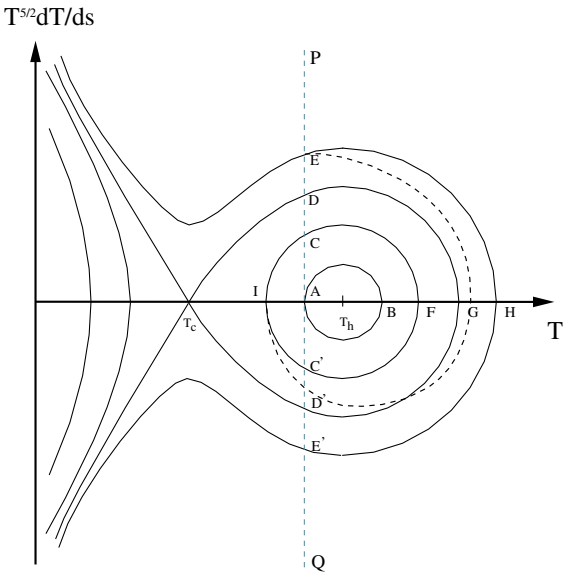

Fig. 1. The form of the phase plane for the solution of Energy Balance Equation. The vertical dotted line illustrates a typical base temperature and the dashed line corresponds to a solution when h has a spatial dependence $\sim \exp(-s/s_*)$.

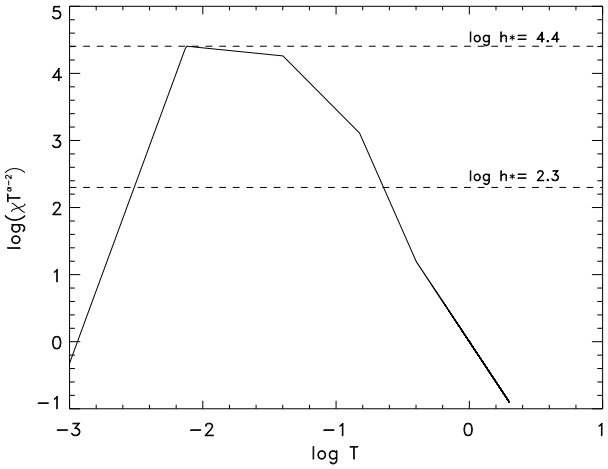

Fig. 2. The relative strengths of the radiation loss term (full line) and the heating term (broken line) in Eq. (5). The temperature is in units of 2×10^6K.

ratio of heating to radiation and s_*, the ratio of the length of the loop to the decay-length of the heating.

Eq. (10) is solved numerically, together with the boundary conditions

$$\frac{dT}{ds} = 0 \qquad \text{at} \qquad summit, \tag{11}$$

$$T = T_b \qquad \text{at} \qquad footpoints.$$

However, before solving the above equations in full, it is helpful to get qualitative information concerning their behaviour, by considering a phase diagram (see Fig. 1) where additionally the heating is assumed to be a constant (Hood and Anzer, 1988; Steele and Priest, 1990).

Setting

$$V = T^{5/2}\frac{dT}{ds}, \tag{12}$$

Eq. (10) becomes

$$\frac{dT}{ds} = VT^{-5/2}, \tag{13}$$

$$\frac{dV}{ds} = L_*^2\left[p^2\chi T^{\alpha-2} - h_*\right], \tag{14}$$

with critical points defined by the conditions

$$V = 0 \qquad \text{and} \qquad T = \left[\frac{h_*}{p^2\chi}\right]^{\frac{1}{\alpha-2}} = T_{crit}.$$

Fig. 2 shows the variation with temperature of $\chi T^{\alpha-2}$ (full lines) and two values of h_* indicated by broken lines. Where the full and broken lines cross (i.e. the two terms on the right hand side of Eq. (14) are equal) a critical point exists. From Fig. 2, is apparent that when $h_* < 10^{4.4}$ two different values of T_{crit} are found.

When $h_* > 10^{4.4}$ no critical point exists. If $h_* < 10^{4.4}$ the saddle point T_c lies at a value of T less than $T_b = 10^{-2}$ (in units of $2 \times 10^6 K$). Therefore, the footpoint lies along the line PQ and, as the temperature gradient is assumed to be positive, it lies between point A and point E. The point corresponding to the loop summit (where $dT/ds = 0$) will lie on the T axis (Fig. 1).

Starting from point A (or a point very close to it) on the phase diagram one finds a hot summit at point B (this solution is known as a hot solution) and a cool summit when contour is extended onwards around the centre point and back to A. Thus, the loop has a cool summit but is hot along part of its length, it is referred to as a hot-cool solution (Hood and Anzer 1988 and Steele and Priest 1990).

Beginning at point C gives a hot solution with a summit at point F and a hot-cool solution with the summit at point I. This existence of both a hot solution and a hot-cool solution will occur for all footpoints between A and D where the hot-cool solution at point T_c has the coolest possible summit temperature for the particular value of h_*. Starting from higher temperature gradient such as at point E, one finds a hot solution with summit at point H but no hot-cool solution. Other possible solutions can be found, such as a cool and warm solution. They are described in Steele and Priest (1990).

When h_* is changed from a value where two critical points exist to another smaller value, the two new critical points are further apart from each other so that the temperature at the saddle point, T_c, and the temperature T_h decrease and increase their values respectively. This effect can be seen in Fig. 3 where the phase diagram with dashed lines corresponds for a smaller value in h_* (only closed contours are shown). Therefore, contours

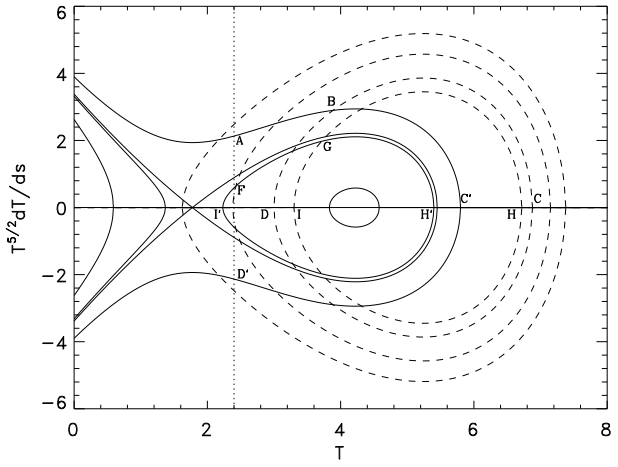

Fig. 3. The form of the phase plane diagram for two different values of h_*. The dashed lines phase diagram corresponds to smaller values of the heating than the solid lines phase diagram. The dotted line indicates a typical boundary temperature. Notice that the temperature and flux scales have been arbitrarily chosen and are for reference only.

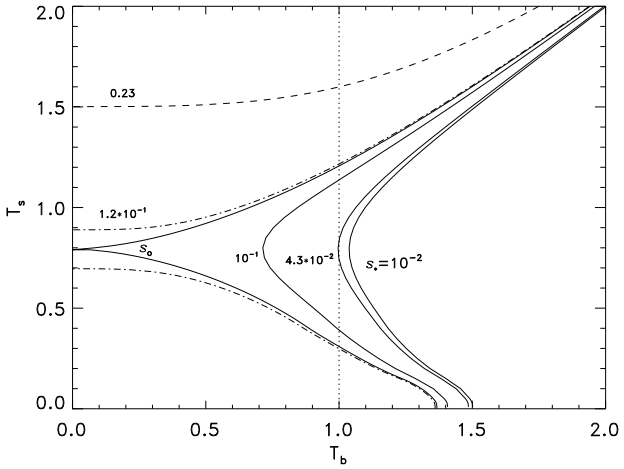

Fig. 4. The summit temperature T_s as a function of the boundary temperature T_b for different values of the decay length of the heating s_*. The dotted line indicates the particular boundary condition $T_b = 1$. The temperatures T_s and T_b are in units of 2×10^6K.

starting with some temperature gradient outside the separatrix in the solid lines phase diagram, are inside the separatrix in the dashed lines phase diagram, such as A moving onwards to B, then one applies an instant variation of the heating to a smaller value in h_* will start moving along the new contours (dashed lines) that are now inside of the separatrix of the new phase diagram, reaching the point C. The solution at this point is hot. However, a cool summit is found when the contour is extended onwards to D.

In the description given above, a hot solution (or hot loops) with the same temperature gradient at the footpoint has a hotter summit when a heating variation is applied. Also, a hot-cool solution is obtained when a heating variation is incorporated. The contour $FGHI$ is a hot-cool loop with summit temperature at I. This case gives a hotter summit than hot-cool loops without heating variation i.e., $FGH'I'$.

On the other hand, when heating is considered to be proportional to $\sim \exp(-s/s_*)$, the same description can be carried out by assuming as a series of instantaneous variations. Therefore, it is found, that an open contour on the phase diagram can be changed into a closed one if the heating decreases along the field line, since the cool temperature T_c is now reduced. This behaviour can be easily seen in Fig. 1 for the dashed line which starts at the point E and finishes at I. In addition, the maximum temperature, no longer at the summit, may increase as T_h increases.

3. Numerical results

In the previous section, the properties of the possible solutions of Eq. (10) were given in terms of phase plane diagrams with the conductive flux being shown as a function of temperature. In this section the numerical solution is sought in order to find the parameter regimes for which they exist. The solution of Eqs. (10) and (11) is governed by the value of the three dimensionless parameters L_*, h_* and s_*.

The presence of the parameter s_* in the heating term of Eq. (10) makes it difficult to study the main characteristic of the solution of this energy equation. However, one can plot the summit temperature (T_s) as a function of the boundary temperature (T_b) in order to visualise the main features of the solutions of Eqs. (10) and (11) when the values of the parameters L_*, h_* and s_* are changed.

Fig. 4 shows the summit temperature T_s as a function of the boundary temperature T_b for $L_* = 4.8 \times 10^{-1}$, and $h_* = 101$. These parameters correspond to a loop length of 6×10^7m and a heating at the base of $10^{-4}\mathrm{Wm}^{-3}$. The different curves are labelled with the corresponding value of s_*. Every point in the curve of this figure corresponds to a static solution, whereas every curve is a family of solutions. The dashed and dashed-dot lines correspond to the family of solutions for which $s_* > s_0$, s_0 being the value of the scale-length for the heating decay for which there is a gap in the values of T_s. That is there are no solutions with these values of T_s. For any value of $s_* < s_0$ there is a minimum value $T_b = T_{bt}$ [turning point at $T_s = T_{st}$] below which solutions of Eqs. (10) and (11) do not exist (Ibañez et al, 1992). Two different solutions exist between $T_{bt}(s_*) < T_b < T_{b0}(s_*)$ (T_{b0} being the value of T_b at which the summit temperature approaches to zero) and one solution when $T_b > T_{b0}(s_*)$. In the upper branch ($T_s > T_{st}$) the summit temperature T_s increases when the boundary temperature T_b increases. On the lower branch, the summit temperature T_s decreases when the boundary temperature T_b increases. Therefore, it is seen in Fig. 4 that the effect of increasing the parameter s_* is to shift the turning point to lower values of T_b.

When one considers the case where a particular boundary condition is taken, for example $T_b = 1$, solutions at equilibrium exist only when $s_* \geq s_{*c}$ ($= 4.3 \times 10^{-2}$). From this value upwards there are two-valued solutions where summit tempera-

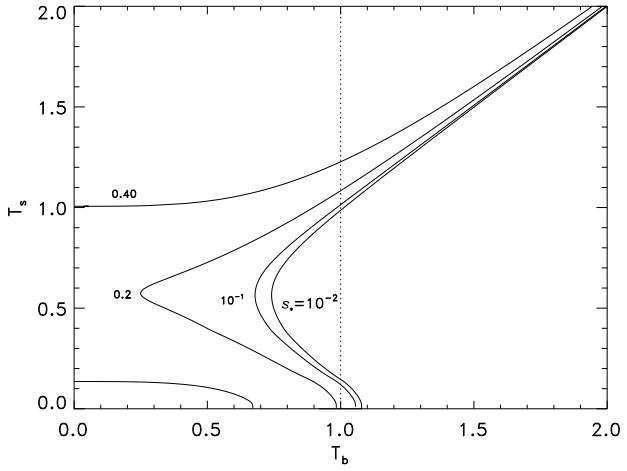

Fig. 5. The summit temperature T_s as a function of the boundary temperature T_b for different values of the decay-length of the heating s_*. The dotted line indicates the particular boundary condition $T_b = 1$. Parameters used are $L_* = 2 \times 10^{-1}$ and $h_* = 1.01 \times 10^2$

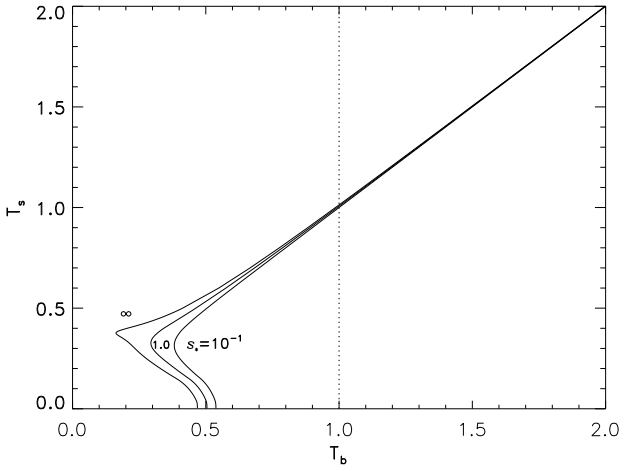

Fig. 6. The summit temperature T_s as a function of the boundary temperature T_b for different values of the decay-length of the heating s_*. The dotted line indicates the particular boundary condition $T_b = 1$. Parameters used are $L_* = 2 \times 10^{-2}$ and $h_* = 1.01 \times 10^2$

ture increases in the upper branch while it decreases in the lower branch. If the value of s_* is increased, there is a value at which a hot solution exists. Very high values of s_* would correspond to a uniform heating, as expected.

The parameter s_* is the heating deposition scale height. When s_* is decreased the heating along the loop is more concentrated at the base of the loop. The input of energy at the summit is then reduced and the energy balance should be established by the thermal conduction. If less energy is supplied into the structure, then the summit temperature of the structure is lowered.

Decreasing even further the value of s_* a critical value is reached and the thermal conduction becomes unable to balance the energy losing and a hot solution does not exist, as far as the static condition is concerned. However, if dynamics is taken into account the structure should evolve to a new equilibrium with a cooler summit (Mendoza and Hood, 1996).

In the Figs. 5 and 6 the summit temperature as a function of the boundary temperature has been plotted for $L_* = 2.0 \times 10^{-1}$ and 2.0×10^{-2} respectively. The main feature observed in Fig. 4 remains, when s_* is varied. The turning points shift to the left when s_* is increased. But these turning points are shifted to lower values of T_s when L_* decreases.

Fig. 5 shows that for a given boundary temperature, for instance $T_b = 1$, solutions are found for any value of s_*. Hence, no critical decay-length of the heating exists. However, by reducing the value of T_b allows the existence of this critical value where thermal non-equilibrium appears (Roberts and Frankenthal, 1980; Priest, 1982).

In Fig. 6 one sees that considering a given boundary temperature $T_b = 1$ only one solution exists for any value of s_*. In addition, a gap is no longer present when s_* is large.

For a given loop structure of small length in contact with a hot boundary the thermal conduction is very effective and will remove any temperature gradient. Therefore, low boundary temperature has to be taken in order to find a critical value of s_*. But, if this value is taken too low, for example, $T_b = 10^{-2}$ (see Fig. 6) no hot solution is found.

A general plot can be drawn by considering the effect of changing the length of the loop and keeping fixed the heating decay-length and the base value of the heating. Fig. 7 shows families of solutions for $s_* = 5 \times 10^{-2}$ and $h_* = 101$, for different values of the length of the loop. The effect of decreasing L_* is to shift the turning points to lower values of T_s and T_b. Therefore, one sees that low temperatures at the base can be obtained when the length of the structure is reduced, when s_* and h_* remain unchanged. Additionally by considering a particular boundary condition $T_b = 1$ one can see that no equilibrium solution exists when L_* is greater than a critical value.

Another important feature of the solution of Eqs. (10) and (11) is the variation of the parameter h_* when s_* and L_* are kept constant. Fig. 8 shows this effect; one may conclude that the effect of changing the value of the parameter h_* is similar to that of changing the parameter s_*, as can be seen in the Fig. 4, where an increase of h_* shifts the turning point to lower values of T_b, and the two branches are separated by a gap when $h_* = h_{*0}$, h_{*0} being the value of the heating at the base where $T_b = 0$.

It has been seen that multiple solutions can be obtained by solving (10) and (11). Cool summits can be found, for example in the Fig. 5 if a parallel line to the T_b-axis is drawn. So, low summit temperatures exist for different values of the decay length s_* but having different boundary temperatures.

In the above $T_s(T_b)$ graphs (Figs. 4-8) there exists a slight bend in the lower branch of the curves, suggesting a lower branch at very low summit temperature. Indeed, it has been found after improving the numerical calculations that this lower branch must exist but it becomes very difficult to resolve numerically.

In Sect. 4 it will be shown that considering a simplified cooling function allows the lower branch to be found. This re-

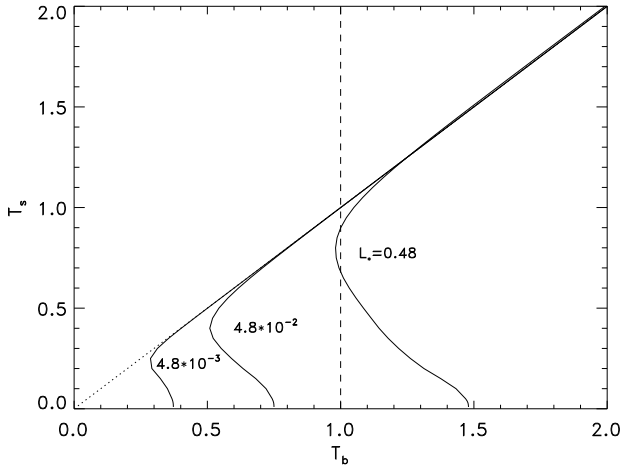

Fig. 7. The summit temperature T_s as a function of the boundary temperature T_b for different values of the loop length L_*. The dashed and dotted lines indicate the particular boundary conditions $T_b = 1$ and $T_b = T_s$, respectively.

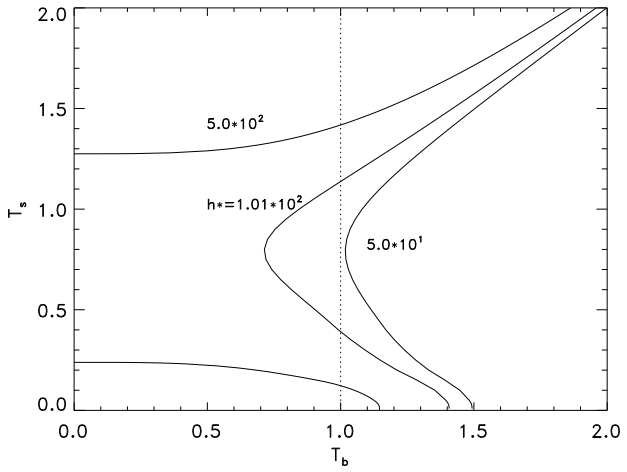

Fig. 8. The summit temperature T_s as a function of the boundary temperature T_b for different values of the heating deposition h_*. The dotted line indicates the particular boundary condition $T_b = 1$. Parameters used are $L_* = 0.48$ and $s_* = 0.1$.

sult confirms that the numerical code cannot resolve the lower branch when the full cooling function is used, but implies that this solution can be found by using another technique, as is shown in the next section, where starting from the known values of low summit temperature one can get the parameters L_*, s_* and h_* that satisfy Eqs. (10) and (11).

3.1. Hot-cool solution

In contrast to Steele and Priest (1990), the heating function used in this work depends explicitly on the position along the loop s. The energy equation cannot be treated as they did because it is now a non-autonomous system. But, one can assume that the temperature and density of the prominence are known and start

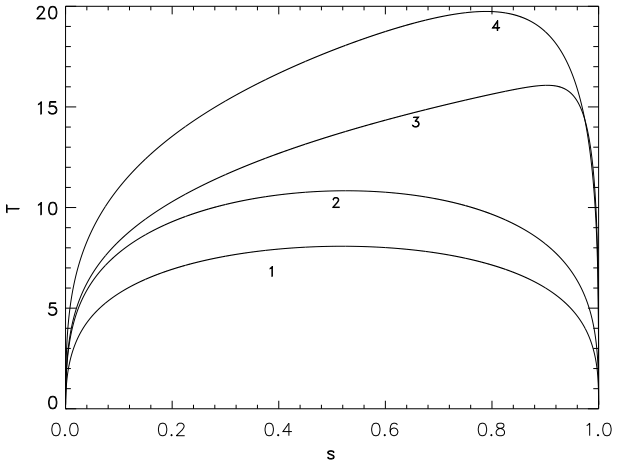

Fig. 9. The variation of temperature T (in units of 10^5K) along a loop from the summit at $s = 0$ to the footpoint at $s = 1$. The numbers refer to the listed values given in Table 1.

the integration of the temperature profile from the summit. Then, in order to explore the hot-cool solution, namely prominence-like solutions, Eq. (10) is integrated from $s = 0$, $T = 0.2$ (in units of $10^5 K$), $dT/ds = 0$, and the integration is continued until $T = 0.2$ (the footpoint temperature is taken at chromospheric values), say at $s = s_1$, then one may set $s' = s/s_1$, to make (10) becomes

$$\frac{d}{ds'}\left(T^{5/2}\frac{dT}{ds'}\right) = L^{'2}\left[\chi T^{\alpha-2} - h' \exp\left(-\frac{1-s'}{s'_*}\right)\right] \quad (15)$$

with $L^{'} = L_* s_1$, $h^{'} = h_* \exp[(1 - 1/s_1)/s_*]$ and $s^{'}_* = s_*/s_1$ and all boundary conditions imposed on Eq. (11) are satisfied but for new parameter values.

Fig. 9 shows the temperature as a function of s when T_b is chosen at the chromospheric value $T_b = 0.2$ for the values of the parameters given in Table 1. All these curves show cool summit temperatures with $T_s = 0.2$ but they are hot along at least part of their length. The maximum temperatures are located between the summit and the footpoint. Using this technique one finds the values of the parameters $L^{'}$, $s^{'}_*$ and $h^{'}$ that produce prominence-like solutions.

In Fig. 9 one sees that when the length of the loop $L^{'}$ is increased the maximum temperature increases and is shifted to the footpoint (it must be remembered that the summit temperature is located at $s = 0$). The latter effect is mainly due to the parameter $s^{'}_*$. When $s^{'}_*$ is small more heat is provided to the footpoint than the summit.

3.2. The effect of a constant total heating

Above we considered the heating function decaying with the distance from the chromosphere along the loop to the summit with the functional form

$$H(s) = h_0 \exp\left(-\frac{1-s}{s_*}\right). \quad (16)$$

Table 1. Parameters obtained for prominence solutions using Eq. (15)

	$L^{'}$	$s_*^{'}$	$h^{'}$	T_{max}
	5.20×10^{-3}	6.27×10^{-2}	3.93×10^{4}	5.48
	1.10×10^{-2}	2.95×10^{-1}	1.11×10^{3}	5.81
	2.21×10^{-2}	1.48×10^{1}	9.86×10^{1}	6.11
	2.76×10^{-2}	1.46×10^{1}	7.89×10^{0}	6.57
	3.05×10^{-2}	1.52×10^{1}	7.12×10^{1}	6.78
	3.59×10^{-2}	9.06×10^{-1}	1.13×10^{2}	7.58
1	5.05×10^{-2}	2.85×10^{0}	5.16×10^{2}	8.08
2	1.29×10^{-1}	1.89×10^{0}	2.34×10^{1}	10.82
	1.30×10^{-1}	3.11×10^{-1}	9.99×10^{1}	12.30
3	1.49×10^{-1}	2.71×10^{-2}	9.45×10^{3}	16.08
	2.31×10^{-1}	8.45×10^{-2}	6.40×10^{2}	17.24
4	3.68×10^{-1}	8.84×10^{-2}	3.75×10^{2}	19.74
	5.32×10^{-1}	9.19×10^{-2}	2.46×10^{2}	21.97
	5.44×10^{-1}	4.49×10^{-2}	8.71×10^{2}	23.09

h_0 had been taken as the heat deposition at the base of the loop and s_* is the free parameter which determines the spatial scale of the heating decay.

The total energy input is not kept constant in the loop when different values of s_* were taken.

Here, an assumption upon this condition is considered and the value of h_0 is chosen such that the total energy input into the loop remains constant.

The value of h_0 is determined by requiring

$$\int_0^1 H(s)ds = \widetilde{H}, \tag{17}$$

where $\widetilde{H}$ is the total dimensionless energy input. Therefore

$$h_0 = \frac{\widetilde{H}}{s_*[1 - \exp(-\frac{1}{s_*})]}. \tag{18}$$

For Alfvén waves the values of $\widetilde{H}$ is

$$1 < \widetilde{H} < 101$$

which corresponds to a rms of velocity amplitude in the range

$$0.58 \text{ km s}^{-1} < \langle \text{v}^2 \rangle^{1/2} < 36 \text{ km s}^{-1}$$

This range is calculated for a loop length of 4×10^7m, $h_0 = 10^{-4}$ Wm^{-3} and a decay-length range

$$10^{-2} < s_* < \infty.$$

We have assumed a coronal density of 10^{-12} kg m^{-3} and an Alfvén speed of 3×10^3 km s^{-1}.

Fig. 10 shows the effect of a constant total heating. The case for $s_* = 0.1$ when total heating is non-constant is indicated with dotted line for comparison.

When s_* is increased the turning point is shifted to the left, as was obtained previously. However, by comparing the two curves for the same values of $s_* = 0.1$ it is seen that for total heating input constant the turning point shifts to lower values of T_b.

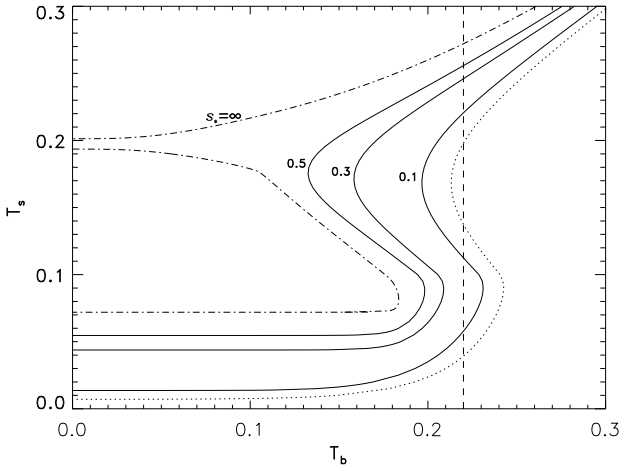

Fig. 10. The summit temperature T_s as a function of the boundary temperature T_b for different values of the decay length of the heating s_*. The dashed line indicates a particular boundary condition. The curve with dotted line corresponds to $s_* = 0.1$, when the total heating is non-constant.

But if a fixed boundary condition is taken, namely $T_b = 0.22$, a hot summit (dotted line) becomes hotter (solid line). A summit temperature in the lower branch also presents an increase in temperature when constant total heating input is considered. However, the summit temperature in the middle branch shows a decrease in temperature.

The increase in temperature in the upper and lower branch is expected when the total energy in the loop is larger and one may identify them as stable solutions. However, the decreasing in the middle branch temperature suggest that those solutions are unstable.

4. Simplified cooling function

This section will discuss the thermal equilibrium of the system (10)-(11) by considering a simplification to the cooling function. The cooling function will be assumed to be a two range piecewise function:

$$Q(T) = \chi T^{\alpha-2} = \begin{cases} T_a^{-7}\, T^{7/2}, & T < T_a, \\ T^{-7/2}, & T > T_a, \end{cases} \tag{19}$$

where T_a is the temperature at which the powers in the radiative loss function change value; for a maximum in the loss function at about 10^5, $T_a = 10^5/T_0$. This function satisfies the basic requirement of the general cooling function, namely that the radiation has a peak at 10^5K. Thus, one expects the qualitative features of the solution to (10) and (11) to carry over when the function (19) is replaced by a more accurate form.

Fig. 11 is a plot of summit temperature as a function of the boundary temperature resulting from the numerical integration of Eq. (10) and (11) for a constant value of the heating term or equivalently a large value of s_*. The different curves are labelled with the corresponding value of L_*^2. As is seen in this figure two points in which all the curves intersect are found at

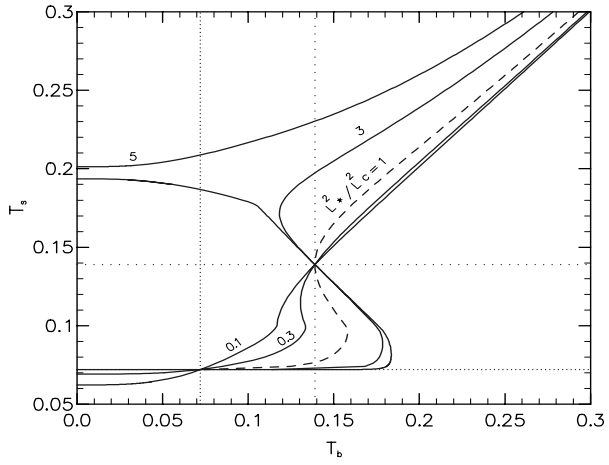

Fig. 11. The summit temperature T_s as a function of the boundary temperature T_b for different values of the loop length L^2_*. The close spaced dot and wide spaced dot lines indicate the two thermal equilibria as a result of $\mathscr{L} = 0$.

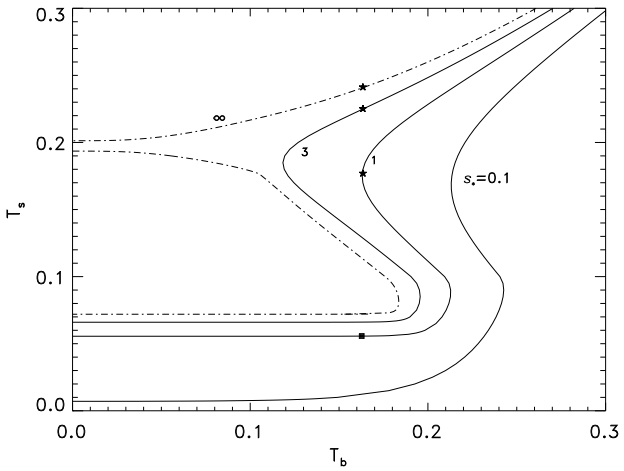

Fig. 12. The summit temperature T_s as a function of the boundary temperature T_b for different values of the decay-length of the heating s_*. The dotted-dashed line corresponds to a uniform heating. The filled star and square indicate the summit temperature at a fixed value of T_b.

T_b = 0.07 and T_b = 0.138. These points correspond to two thermal equilibrium states given by the solutions of $\mathscr{L}$ = 0 (=cooling-heating).

For L^2_* small ($< 0.1L^2_c$) the relation $T_s(T_b)$ is a single-valued function while for $L^2_* > L'^2_c$ ($\approx 0.1L^2_c$) it becomes a three valued function with an S-type characteristic. In particular, at $T_b = T_e$, T_e being the temperature at equilibrium (in this case T_e = 0.138) and for $L^2_* > L'^2_c$ ($\approx 0.39L^2_c$), the multiple solutions are the thermal equilibrium state and two additional states in nonthermal equilibrium. For large values of L^2_* ($L^2_* > L^2_{*0}$, L^2_{*0} being the value for which T_b = 0 at the turning point) a gap for the summit temperature T_s appears where no solution exists.

For values of $L^2_* < L'^2_c$ the summit temperature is a monotonically increasing function of T_b. For any value of L^2_* in the range $L'^2_c < L^2_* < L^2_{*0}$, however, there are two turning points (or catastrophe points) that divide the curve $T_s(T_b, L^2_*)$ in the branches corresponding to three different solution of Eqs. (10) and (11). In the upper and lower branches, the summit temperature T_s increases when the boundary temperature T_b increases, and in the middle branch the summit temperature decreases when the boundary temperature increases.

When $L^2_* > L^2_{*o}$ only the lower turning point remains, and it separates the middle and lower branches and, as was pointed out above, a gap for T_s exists. The width of such a gap increases when L^2_* increases. When the value of L^2_* is considered to be equal to L^2_c (the dashed curve in Fig. 11) one can see that the upper turning point coincides with the temperature at thermal equilibrium. This value of L^2_* is the critical one found in the Sect. 5.1 below making use of a simple first order stability analysis.

Fig. 12 shows several families of the static solution for $L^2_* = 5L^2_c$ and the labelled values of s_*. The dotted-dashed line is the family of static solutions when the heating is considered constant or s_* is very large. It reproduces the general trends that have been shown previously, including the gap. If s_* is decreased the gap disappears and the turning point is shifted to the right hand side. When s_* is decreased one can observe that the lower branch in those curves are shifted to lower values of T_s as expected. The filled star and square in Fig. 12 correspond to the solution of Eq. (10) with (11) for a particular value T_b. It can be seen how the temperature at the summit decreases with decreasing s_*. Here one can assume that the thermal structure at coronal temperatures evolves through a sequence of equilibria that satisfy the energy equation (10). If s_* is very small (as has been described previously), no static solution exists for that particular T_b and the thermal structure will evolve to an equilibrium with a lower temperature at the summit (at a value of T_s shown with a filled square).

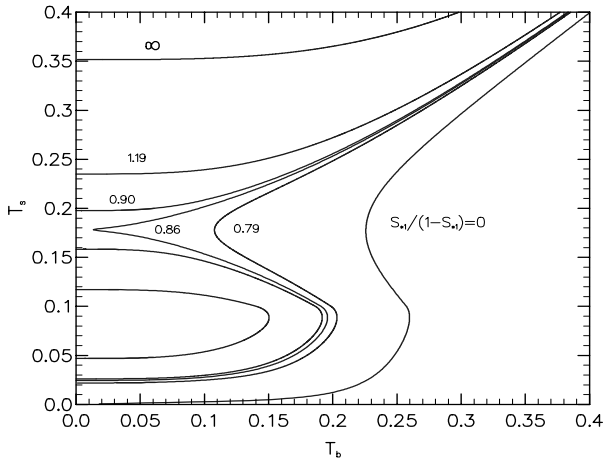

Fig. 13. The summit temperature T_s as a function of the boundary temperature T_b for different values of the ratio $s_{*1}/(1 - s_{*1})$.

Fig. 13 shows the summit temperature as a function of boundary temperature for different values of the ratio of $s_{*1}/(1-s_{*1})$ when a step function form of the heating is considered as

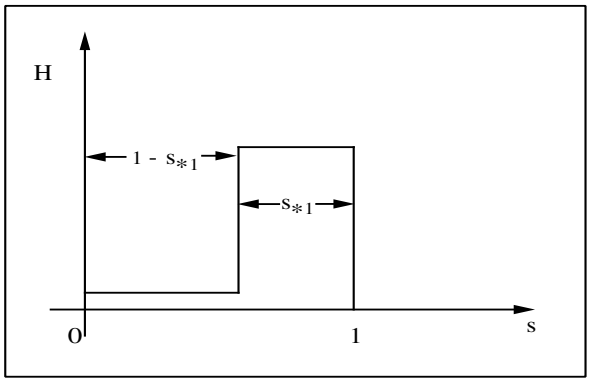

Fig. 14. Schematic functional form for the spatial dependence of the heating function.

shown in Fig. 14. In Sect. 3.2 a phase plane diagram for two different values of h_* was described and analysed qualitatively to find what happened to the solution when an instant variation of the heating was applied. When s_{*1} is increased from 0 to 1 one can observe the same general effect studied previously with the exponential variation of the heating.

5. The stability of the static solutions

In the previous sections, static solutions of the energy equation were obtained. Multiple solutions for given values of the parameters and boundary conditions were found. Now, an interesting problem would be to study the stability of the static solutions of the energy equation. In order to determine the stability of a given equilibrium (or static solution), the method proposed by Landau (1944) for studying turbulence will be used (see also Drazin and Reid 1981; Ibañez, Parravano and Mendoza 1993; Ibañez and Rosenzweig 1995).

The aim of this method is to examine the conditions prevailing just at the onset of the nonlinear regime and to analyse the scope of the well-known linear criteria for thermal instability, instead of following the evolution of a particular thermal structu re during a well advanced stage of the nonlinear regime.

One assumes that the dimensionless time-dependent energy equation at constant pressure ($p = 1$),

$$\frac{\partial T}{\partial t} = T\left\{\frac{\partial}{\partial s}\left(T^{5/2}\frac{\partial T}{\partial s}\right) - L_*^2(\chi T^{\alpha-2} - H)\right\} \tag{20}$$

has solutions of the form

$$T(s,t) = \overline{T}(s) + \delta T(s,t), \tag{21}$$

$$\delta T(s,t) = \sum_{i=1}^{\infty} A^i(t) f_i(s), \tag{22}$$

$$\frac{d \mid A(t) \mid}{dt} = \sum_{i=1}^{\infty} a_i \mid A(t) \mid^i, \tag{23}$$

where $\overline{T}(s)$ is the solution to the static equation

$$\frac{\partial}{\partial s}\left(T^{5/2}\frac{\partial T}{\partial s}\right) - L_*^2(\chi T^{\alpha-2} - H) = 0 \tag{24}$$

with boundary conditions

$$\begin{aligned} &\frac{\partial T}{\partial s} = 0 \qquad \text{at} \qquad s = 0 \quad \text{(summit)},\\ &T = T_b \qquad \text{at} \qquad s = 1 \quad \text{(boundary)}, \end{aligned} \tag{25}$$

$A(t)$ is a function of time, and $f_i(s)$ are functions of the coordinate s that satisfy the boundary conditions

$$\begin{aligned} &\frac{df_i}{ds} = 0 \qquad \text{at} \qquad s = 0,\\ &f_i(s) = 0 \qquad \text{at} \qquad s = 1. \end{aligned} \tag{26}$$

Both $A(t)$ and $f_i(s)$ are to be determined. Strictly speaking, the series (22) and (23) contain an infinite number of terms. In practice, however, the first few terms are enough to examine the stability near the critical states.

5.1. First-order approximation

If $\overline{T} = T_e$ is a trivial solution, the linear analysis of stability can be carried out analytically. In fact, substituting (21) and (22) in Eq. (20) and setting terms of first order in A equal, one obtains the equation

$$\frac{d^2 f_1}{ds^2} + \frac{1}{T_e^{7/2}}\left(-(\alpha-2)L_*^2\chi T_e^{\alpha-2} - a_1\right) f_1 = 0 \tag{27}$$

with boundary conditions

$$\begin{aligned} &\frac{df_1}{ds} = 0 \qquad \text{at} \qquad s = 0,\\ &f_1(s) = 0 \qquad \text{at} \qquad s = 1. \end{aligned} \tag{28}$$

The solutions of Eq. (27) - (28) are

$$f_1(s) = \cos[(2N-1)\frac{\pi}{2}s] \tag{29}$$

where $N = 1, 2, ...$

On the other hand, $A(t)$ in Eq. (23) up to first order becomes

$$A(t) = A_0 e^{a_1 t} \tag{30}$$

where the growth rate a_1 is given by

$$a_1 = -(\alpha-2)L_*^2\chi T_e^{\alpha-2} - b_N^2 T_e^{7/2} \tag{31}$$

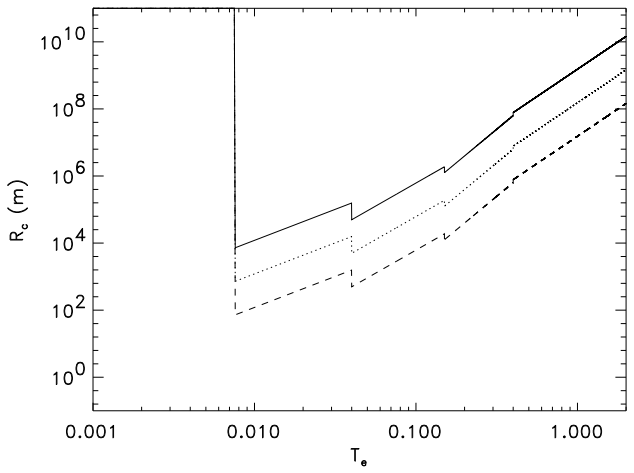

Fig. 15. Critical dimension of the structure as a function of temperature T_e (in units of 2×10^6K) separating regions of thermal stability and instability. The oblique solid, dotted and dashed line, correspond to a plasma at pressure p_0 = 0.01, 0.1 and 1.0 pascals respectively.

A_o is a constant, T_e is any solution of the equation $\mathscr{L} = 0$, and b_N is $(2N-1)\pi/2$, respectively.

From Eqs. (30) and (31) one concludes that the thermal structure is thermally stable ($a_1 < 0$) if

$$-(\alpha-2)L_*^2\chi T_e^{\alpha-3} - b_N^2 T_e^{5/2} < 0. \tag{32}$$

For the two range cooling function and Hildner's cooling function, the thermal equilibrium is absolutely stable if $(2-\alpha)$ is negative as far as the linear approximation is concerned. But for $(2-\alpha) > 0$ the trivial solution becomes unstable provided that

$$L_*^2 > \frac{b_N^2}{-(\alpha-2)\chi T_e^{\alpha-11/2}}. \tag{33}$$

On the other hand, when the instability sets in the fastest growing mode is the fundamental one (N = 1), for which Eq. (31) defines a critical value of L_*^2 for the marginal state (a_1 = 0) i.e.

$$L_*^2 = L_c^2 \equiv \frac{b_1^2}{(2-\alpha)\chi T_e^{\alpha-11/2}}, \tag{34}$$

Note that L_c defined by Eq. (34) has physical meaning only if $2-\alpha > 0$. For the simplified cooling function $(2-\alpha) > 0$ corresponds to $T > T_a$, therefore the critical value for the marginal state is $L_c^2 = \pi^2 T_e^7/14$.

Therefore, if $L_*^2 > L_c^2$, a_1 is positive and the solution is unstable.

From the definition of L_* (Eq. (7))

$$L_*^2 = \frac{L_0^2\tilde{\mu}^2 p_0^2 \chi_0 T_0^{\alpha-11/2}}{\mathscr{R}^2\kappa_0} \tag{35}$$

and Eq. (34) one can determine the critical dimension for marginally stable homogeneous structures in thermal equilibrium as :

$$R_c = \frac{\mathscr{R} b_1}{\tilde{\mu} p_0}\left[\frac{\kappa_0}{(2-\alpha)\chi_0\chi T_e^{\alpha-11/2}T_0^{\alpha_0-11/2}}\right]^{1/2}. \tag{36}$$

Structures longer than R_c will be thermally unstable.

Fig. 15 shows R_c as a function of temperature according to Eq. (36), for pressures p_0 = 0.01, 0.1, 1.0 pascals. For a temperature between $\sim 1.5 \times 10^4$ and 10^6 K, perturbations on the scale-size below the diagonal broken line are stable. The broken shape of this line is due to the piecewise nature of the radiation cooling function. In the range of $T < 1.5 \times 10^4$ K perturbations are stable since that $(2-\alpha) < 0$.

5.2. Second-order approximation

For the trivial solution T_e, substituting (21) and (22), and setting terms of second order in A equal, one obtains Eq.

$$\frac{d^2 f_2}{d\tilde{s}^2} + \omega^2 f_2 = -\frac{5}{2T_e} + \frac{a_2}{b_N^2 T_e^{7/2}}\cos\tilde{s}$$
$$+\left\{\frac{6}{T_e} + \frac{L_*^2(\alpha-2)\chi T_e^{\alpha-3}}{b_N^2 T_e^{7/2}}\left[1+\frac{1}{2}(\alpha-3)\right]\right\}\cos^2\tilde{s} \tag{37}$$

with the boundary conditions

$$\begin{aligned} \frac{df_2}{d\tilde{s}} &= 0 \qquad \text{at} \qquad \tilde{s} = 0, \\ f_2(\tilde{s}) &= 0 \qquad \text{at} \qquad \tilde{s} = \frac{\pi}{2}, \end{aligned} \tag{38}$$

where $\tilde{s} = (\pi/2)s$ $\omega^2 = 2 + L_*^2(\alpha-2)\chi T_e^{\alpha-11/2}/b_N^2$ and $b_N = (2N-1)\pi/2$. As is well known, the fundamental mode N = 1 is the fastest growing mode.

The general solution of Eq. (37) with boundary conditions (38) is

$$\begin{aligned} f_2(\tilde{s}) \;=\; & -\frac{5}{2T_e\omega^2}(1-\cos\omega\tilde{s}) \\ & + \frac{a_2}{b_1^2 T_e^{7/2}(\omega^2-1)}(\cos\tilde{s}-\cos\omega\tilde{s}) + \frac{1}{\omega^2(\omega^2-4)} \\ & \left[\left(\frac{6}{T_e}\right) + \frac{L_*^2(\alpha-2)\chi T_e^{\alpha-3}[1+\frac{1}{2}(\alpha-3)]}{b_1^2 T^{7/2}}\right] \\ & \times \left[(2-\omega^2)\cos\omega\tilde{s} + \omega^2\cos^2\tilde{s} - 2\right] + \overline{c_1}\cos\omega\tilde{s}, \end{aligned} \tag{39}$$

where $\overline{c_1}$ is an arbitrary constant and

$$a_2 \;=\; T_e^{7/2} b_1^2 \frac{(\omega^2-1)}{\cos(\frac{\pi}{2}\omega)}\left\{\frac{5}{2T_e\omega^2}[1-\cos(\frac{\pi}{2}\omega)] + \frac{1}{\omega^2(\omega^2-4)}\right.$$

$$\left[\left(\frac{6}{T_e}\right)+\frac{L_*^2(\alpha-2)\chi T_e^{\alpha-3}[1+\frac{1}{2}(\alpha-3)]}{b_N^2 T^{7/2}}\right]$$
$$\times\left[(2-\omega^2)\cos\frac{\pi}{2}\omega-2\right]+\overline{c_1}\cos(\frac{\pi}{2}\omega)\Big\} \quad (40)$$

is the Landau constant.

Close to the marginal state, defined by Eq. (34), Eqs. (39) and (40) simplify to

$$f_2(\tilde{s}) = -\frac{5}{2T_e}(1-\cos\tilde{s}) - \frac{a_2}{2L_*^2(\alpha-2)\chi T_e^{\alpha-2}}\tilde{s}\sin\tilde{s}$$
$$-\frac{1}{3}\left(\frac{5}{T_e}-\frac{(\alpha-3)}{2T_e}\right)(\cos\tilde{s}+\cos^2\tilde{s}-2)+\overline{c_1}\cos\tilde{s} \quad (41)$$

$$a_2 = -\frac{2}{3b_N}L_*^2(\alpha-2)\chi T_e^{\alpha-2}\left(-\frac{5}{2T_e}+\frac{(\alpha-3)}{T_e}\right) \quad (42)$$

respectively.

On the other hand, from the integration of Eq. (23) up to the second-order, one obtains

$$A(t) = A_0\left[-\left(\frac{a_2}{a_1}A_0\right)+\left(1+\frac{a_2}{a_1}A_0\right)e^{-a_1 t}\right]^{-1} \quad (43)$$

A_0 being the value of $A(t)$ at $t = 0$.

As is well-known, for $L_*^2 > L_c^2$ ($a_1 > 0$), supercritical stability (Landau, 1944; Drazin and Reid, 1981) sets in when $a_2 < 0$. Then, the trivial solution becomes linearly unstable, but it tends to a new static solution eventually because the amplitude $A(t)$ equilibrates to $A_e = \mid a_1 \mid / \mid a_2 \mid$ when $t \to \infty$. Therefore, as follows from Eq. (43), the perturbation saturates to the value A_e as $t \to \infty$, i.e., the uniform thermal structure smoothly evolves to a nonuniform static state. On the other hand, subcritical instability occurs when $a_2 > 0$ and $a_1 < 0$ ($L_*^2 < L_c^2$). In this case, $A(t) \to 0$ as $t \to \infty$ if $A_0 < A_e$ (threshold value). But, if $A_0 > A_e$ the solution (42) breaks down at the time

$$t_2 = \frac{1}{\mid a_1 \mid}\ln\frac{A_0/\mid A_e \mid}{\mid 1-(A_0/\mid A_e \mid)\mid} \quad (44)$$

Obviously, first-order disturbances $f_1(s) = -\cos\pi s/2$ also are solutions to Eq. (27), and the corresponding second-order analysis leaves a change of sign for a_2, i.e. if the loop under consideration is supercritically stable for disturbances increasing the summit temperature, it becomes superexponentially unstable for disturbances decreasing the summit temperature, as far as the second approximation holds.

Additionally, one may conclude that when loops in thermal equilibrium are subcritically unstable ($a_1 < 0, a_2 > 0$) for positive first-order disturbances (or increasing the summit temperature), they will be asymptotically stable for negative disturbances (or decreasing the summit temperature) (see Table 2).

In Fig. 11, for the upper thermal equilibrium solution $T = T_e$, one finds that close to L_c^2 for $L_*^2 < L_c^2$ ($a_1 < 0$), for positive disturbances, $a_2 < 0$, but for negative disturbances, $a_2 > 0$. Therefore, the above solution is asymptotically stable for positive disturbances, and subcritically unstable for negative disturbances, with a threshold value for the amplitude given by $\mid a_1 \mid / \mid a_2 \mid$, i.e. the loop is stable with respect to an increase in its temperature, but it cools down catastrophically when it suffers large enough negative disturbances. For $L_*^2 > L_c^2$ ($a_1 > 0$), $a_2 < 0$ for positive disturbances. Therefore, the solution T_e is supercritically stable and will evolve towards its saturated states, i.e. to stable solutions. For negative disturbances $a_2 > 0$, the structure becomes superexponentially unstable, i.e. when one increases the temperature of the loop the structure goes to an inhomogeneous solution, but when the temperature is reduced the loop cools down catastrophically. The above result shows the evolutionary tendency in the neighbourhood of the thermal equilibrium solution T_e. It is obvious that a higher order of approximation would be required to follow the above evolution.

The above considerations on the stability of the trivial solution suggest that the positive slope branches (upper and lower branches) on the plane (T_s, T_b) are stable solutions and the middle negative slope branch as the locus of the unstable static solutions of (24) and (25). Therefore, supercritical stability and subcritical instability appear when the relation $T_s(T_b)$ shows turning points. Otherwise, the structure is absolutely stable as is apparent from Fig. 11 for $L_*^2 < 0.3L_c^2$.

Table 3 summarises the behaviour of the thermal stability for the different ranges in the piecewise cooling function given by Hildner (1974). The first column gives the corresponding interval of temperature and the second one is the rate resulting from the linear analysis. The third and fourth columns give the corresponding sign of the Landau constant for positive and negative disturbances of temperature, respectively. Therefore, for temperature less than 1.5×10^4 the loop is overheated for an increase in its temperature but is thermally stable for disturbances smaller than the threshold value ($\mid a_1 \mid / \mid a_2 \mid$), for a decrease in its temperature. Instead, for $T > 1.5 \times 10^4$ the loop supercritically saturates, for an increase in its temperature but for a decrease, the loop superexponentially cools down.

Table 2. Definition for the combination between sign of a_1 and a_2.

a_1	a_2	Definition
−	−	Asymptotical Stability
−	+	Subcritical Instability
+	−	Supercritical Stability
+	+	Superexponential Instability

Table 3. Nature of the thermal stability for the different ranges in Hildner's cooling function.

T (K)	a_1	a_2^+	a_2^-
$< 1.5 \times 10^4$	−	+	−
$1.5 \times 10^4 - 8.0 \times 10^4$	+	−	+
$8.0 \times 10^4 - 3.0 \times 10^5$	+	−	+
$3.0 \times 10^5 - 8.0 \times 10^5$	+	−	+
$8.0 \times 10^5 - 10^7$	+	−	+

Note that while the linear analysis of thermal equilibrium may predict thermal stability, the second order analysis allows one to deduce how the structure evolves once it becomes linearly unstable.

6. Conclusions

In this paper the static solutions of thermal equilibrium at constant pressure along a symmetric coronal loop have been investigated. Here, a special coronal heating function, which depends only on the spatial variable, has been considered. These solutions have been initially identified by using a phase diagram technique. The phase diagram, under consideration of spatially dependent heating function, represents a non-autonomous system. It was seen that a prominence-like condensation can be produced when a reduction of the heating along the field lines is applied.

Furthermore, the static solutions were studied numerically and the effect of the parameters L_*, h_* and s_* were analysed. It was found that there is a critical value of the decay-length of the heating and the base value of the heating, below which thermal equilibrium with a hot summit does not exist. This lack of thermal equilibrium is also present when the length of the field line is greater than a critical value. Hood and Priest (1979), Roberts and Frankenthal (1980) and Priest (1982) have been concerned with this kind of feature, suggesting that the system will evolve quasi-statically to a cool solution because of the catastrophic cooling. Based on this fact, and because the graphs $T_s(T_b)$ showed an apparent bend in the lower branch, attention was focussed on investigating the prominence-like solutions. The prominence properties, namely temperature and pressure were considered, and the thermal profiles were calculated by integrating the energy equation from the loop apex to the footpoint, from which the parameters L_*, h_* and s_* were determined.

On the other hand, a simplified cooling function was considered and this allowed us to demonstrate that the lower branch exists. However, the lower branch is not easily resolved numerically for a more accurate cooling function, such as the one given by Hildner (1974). It is expected that the same results would be obtained when more recent cooling functions (Athay, 1986; Cook et al. 1989) are employed.

The stability of the uniform static solutions of the energy equation were studied up to the second order approximation, the results suggesting that for the S-shaped type configuration in the graph $T_s(T_b)$ the upper and lower branches are stable and the middle branch is unstable. In addition, it was concluded that the linear approximation predicts that the instability depends on the size of the structure, but the second order approximation predicts that the stability or instability, additionally depends on the size of the structure and also whether the disturbance decreases or increases the initial temperature.

Finally, the effect of the spatial variation was studied, of the heating but keeping the total energy input of the loop constant. The results found in this case showed similar behaviour to those found when the total energy input was not kept constant when s_* was varied.

Other forms of spatial heating can be considered but, if the maximum of the heating is near the footpoints, our conclusions will carry over.

Acknowledgements. The authors would like to thank U. Anzer for the helpful comments for improving this revised version. CAMB gratefully acknowledges Prof. M. Ibañez for discussing particular points.

References

Athay, R.G. 1986, AJ 308, 975
Cook, J.W., Cheng, C.C., Jacobs, V.L. and Antiochos, S.K. 1989, AJ 338, 1176
Craig, I.L., McClymont, A.N. and Underwood, J.H. 1978, A&A 70, 1
Drazin, P.G. and Reid, W.H. 1981, Hydrodynamic Stability, Cambridge University Press, Cambridge
Hildner, E. 1974, Solar Phys. 35, 123
Hood, A.W. and Anzer, U. 1988, Solar Phys. 115, 61
Hood, A.W. and Priest, E. R. 1979, A&A 77, 233
Ibañez, S.M.H., Parravano, A. and Mendoza, B.C.A. 1992, AJ 398, 177
Ibañez, S.M.H., Parravano, A. and Mendoza, B.C.A. 1993, AJ 407, 611
Ibañez, S.M.H. and Rosenzweig, P. 1995, Phys. Plasmas 2, 4127
Landau, L. 1944, C.R. Acad. Sci. 44, 311
Mendoza-Briceño, C.A. 1996, PhD Thesis, University of St. Andrews, St. Andrews, Scotland
Mendoza, C.A. and A.W. Hood 1996, Astro. Lett. and Communications 34, 107
Priest, E.R. 1982, Solar Magnetohydrodynamics, D. Reidel Publ. Co., Dordrecht, Holland
Priest, E.R. and Smith, E.A. 1979, Solar Phys. 64, 267
Roberts, B. and Frankenthal, S. 1980, Solar Phys. 68, 103
Rosner, R., Tucker, W.H. and Vaiana, G.S. 1978, AJ 220, 643
Serio, S., Peres, G., Vaiana, G.S., Golub, L. and Rosner, R. 1981, AJ 243, 288
She, Z. S., Malherbe, J. M. and Raadu, M. A.: 1986, A&A 164, 364.
Spitzer, L.: 1962, Physics of Fully Ionised Gases, 2nd edition, Willey Interscience, New York.
Steele, C. D. C. and Priest, E. R.: 1990a, Solar Phys. 125, 295.
Steele, C. D. C. and Priest, E. R.: 1994, A&A 292, 291.
Vesecky, J. F., Antiochos, S. K. and Underwood, J. H.: 1979, AJ 233, 987.
van den Oord, G. H. J. and Zuccarello, F.: 1996 A&A Submitted.
Wragg, M. A. and Priest, E. R.: 1981a, Solar Phys., 69, 257.
Wragg, M. A. and Priest, E. R.: 1981b, Solar Phys., 70, 293.
Wragg, M. A. and Priest, E. R.: 1982, Solar Phys., 80, 309.

This article was processed by the author using Springer-Verlag LaTeX A&A style file *L-AA* version 3.